Supporting information

Polynuclear Cu(I) and Ag(I) Phosphine Complexes Containing multi-dentate polytopic ligands: Synthesis, Crystal Structures and Photoluminescence Properties

Jing Xiang,[a,*] Shun-Cheung Cheng,[b] Xin-Xin Jin,[a] Qian-Qian Su,[a] Xin Zhou,[a] Wing-Kin Chu,[b,] Chi-Fai Leung,[c,*] and Chi-Chiu Ko[b,*]

[a] *College of Chemistry and Environmental Engineering, Yangtze University, Jingzhou 434020, Hubei, P. R. China. Email: xiangjing@yangtzeu.edu.cn*

[b] *Department of Chemistry, Institute of Molecular Functional Materials, City University of Hong Kong, Tat Chee Avenue, Kowloon Tong, Hong Kong, China*

[c] *Department of Science and Environmental Studies, The Education University of Hong Kong, 10 Lo Ping Road, Tai Po, Hong Kong, China*

Table of supporting information

	Experimental section	3
Figure S1	^{1}H NMR spectroscopy of **1**	4
Figure S2	^{31}P{^{1}H} NMR spectroscopy of **1**.	4
Figure S3	The π···π stacking interactions in **1** (a), **2**(b), **3**(c) and **4** (d).	5
Figure S4	UV spectra of ligands $\mathbf{L^1}$, $\mathbf{H_2L^2}$ and $\mathbf{H_3L^3}$ in MeCN.	5
Figure S5	The emission spectra of compounds **1** and **3** in CH_2Cl_2 (λ_{ex} = 400 nm)	5
Figure S6	Emission spectra of **3** in the solid state (a) and in 77 K EtOH-MeOH (4:1, v/v) glassy state (b).	6
Figure S7	Emission spectra of **6** in the solid state (a) and in 77 K EtOH-MeOH (4:1, v/v) glassy state (b).	6
Table S1	Predicted transition energies and the changes in the electron densities of the lowest 10 vertical transitions of compound **1**.	7
Table S2	Predicted transition energies and the changes in the electron densities of the lowest 10 vertical transitions of compound **3**.	8
Table S3	Predicted transition energies and the changes in the electron densities of the lowest 10 vertical transitions of compound **4**.	9
Table S4	Predicted transition energies and the changes in the electron densities of the lowest 10 vertical transitions of compound **5**.	10
Table S5	Predicted transition energies and the changes in the electron densities of the lowest 10 vertical transitions of compound **6**.	11
Figure S8.	Overlaid experimental (black) and predicted (red) electronic absorption spectra of **3** - **6** in dichloromethane. The predicted vertical transitions were shown as red vertical bars with height equal to their calculated oscillator strengths.	12

Experimental section

Physical Measurements and Instrumentation. ^{1}H NMR and $^{31}P\{^{1}H\}$ NMR spectra were recorded on a Bruker AV300 (300 MHz) FT-NMR spectrometer. Chemical shifts (δ, ppm) are reported relative to tetramethylsilane (Me_4Si). Elemental analysis was performed on an ElementarVario MICRO Cube elemental analyzer. IR spectra of the solid samples as KBr discs were obtained within the range 4000–400 cm^{-1} on an AVATAR 360 FTIR spectrometer. All of the electronic absorption spectra were recorded on a Hewlett–Packard 8453 or Hewlett–Packard 8452A diode-array spectrophotometer. Steady-state emission spectra were measured at room temperature and at 77 K on a Horiba JobinYvon Fluorolog-3-TCSPC spectrofluorometer. The solutions were rigorously degassed on a high-vacuum line in a two-compartment cell with not less than four successive freeze–pump–thaw cycles. The measurements at 77 K were carried out on dilute solutions of the samples in EtOH/MeOH (4:1, v/v) loaded in a quartz tube inside a quartz-walled Dewar flask that contained liquid nitrogen. Luminescence lifetimes were measured by using the time-correlated single-photon-counting (TCSPC) technique on a Fluorolog-3-TCSPC spectrofluorometer in a fast MCS mode with a Nano LED-375 LH excitation source, which had a peak excitation wavelength at 375 nm and a pulse width of less than 750 ps. The photon-counting data were analyzed on Horiba JobinYvon Decay Analysis Software.

X-ray Crystallography. The crystal structures were determined on an Oxford Diffraction Gemini S Ultra X-ray single-crystal diffractometer using graphite-monochromated Cu K_a radiation (λ = 1.5417 Å). The structures were solved by using direct methods with the SHELXS-97 program.[1] The Cu, Ag metal atoms and many of the non-hydrogen atoms were located according to the direct methods. The positions of the other non-hydrogen atoms were located after refinement by full matrix least-squares by using the SHELXL-97 program.[2] In the final stage of the least-squares refinement, all non-hydrogen atoms were refined anisotropically. H atoms were generated by SHELXL-97 program. The positions of H atoms were calculated based on riding model with thermal parameters that were 1.2 times that of the associated C atoms and participated in the calculation of the final R indices. Crystallographic data (including structure factors) of the structures reported in this paper have been deposited to the Cambridge Crystallographic Data Centre (CCDC) with the depository numbers CCDC 1577074-1577079.

Computational Details. All the calculations were done by GAUSSIAN 09, version B.01.[3] The ground state and lowest triplet state structures of complexes **1** - **6** were optimized using B3LYP functional[4] and a mixed basis set of 6-31+G(d) (for C, H, N, P) and LANL2DZ[5] (for Cu and Ag). To reduce computation complexity, the phenyl rings of the triphenylphosphine ligands are replaced by methyl groups. Polarized Continuum Model[6] (PCM) was employed to account for the solvent effect of dichloromethane. Frequency calculations were done after optimization and no imaginary frequencies were found. The vertical electronic transitions of 1, 3 - 6 were calculated by time-dependent density functional theory.[7] The X-ray crystal structures of the complexes were used without further optimization.

Reference:

(1) G. M. Sheldrick, SHELX-97: Programs for Crystal Structure Analysis, release 97-2, University of Gottingen, Germany, 1997.
(2) A. Altomare, G. Cascarano, C. Giacovazzo, A. Guagliardi, M. Burla, G. Polidori and M. Camalli, *J. Appl. Crystallogr.*, 1994, **27**, 435.
(3) M. J. Frisch, G. W. Trucks, H. B. Schlegel *et al.*, *Gaussian 09*, Revision B.01, Gaussian, Inc., Wallingford CT, 2009
(4) (a) A. D. Becke, *J. Chem. Phys.* 1993, **98**, 5648-5652; (b) C. Lee, W, Yang, R. G. Parr, *Phys. Rev. B*, 1988, **37**, 785; (c) P. J. Stephens, F. J. Devlin, C. F. Chabalowski, M. J. Frisch, *J. Phys. Chem.* 1994, **98**, 11623-11627.
(5) (a) Y. Zhao and D. G. Truhlar, *Theor. Chem. Acc.*, 2008, **120**, 215–241; (b) A. Schäfer, H. Horn and R. Ahlrichs, *J. Chem. Phys.* 1992, **97**, 2571–2577; (c) W. R. Wadt and P. J. Hay, J. Chem. Phys. 1985, 82, 284–298.
(6) G. Scalmani and M. J. Frisch, *J. Chem. Phys.* 2010, **132**, 114110.
(7) (a) R. Bauernschmitt, R. Ahlrichs, *Chem. Phys. Lett.*, 1996, **256,** 454-64; (b) G. Scalmani, M. J. Frisch, B. Mennucci, J. Tomasi, R. Cammi, V. Barone, *J. Chem. Phys.*, 2006, **124**, 094107.

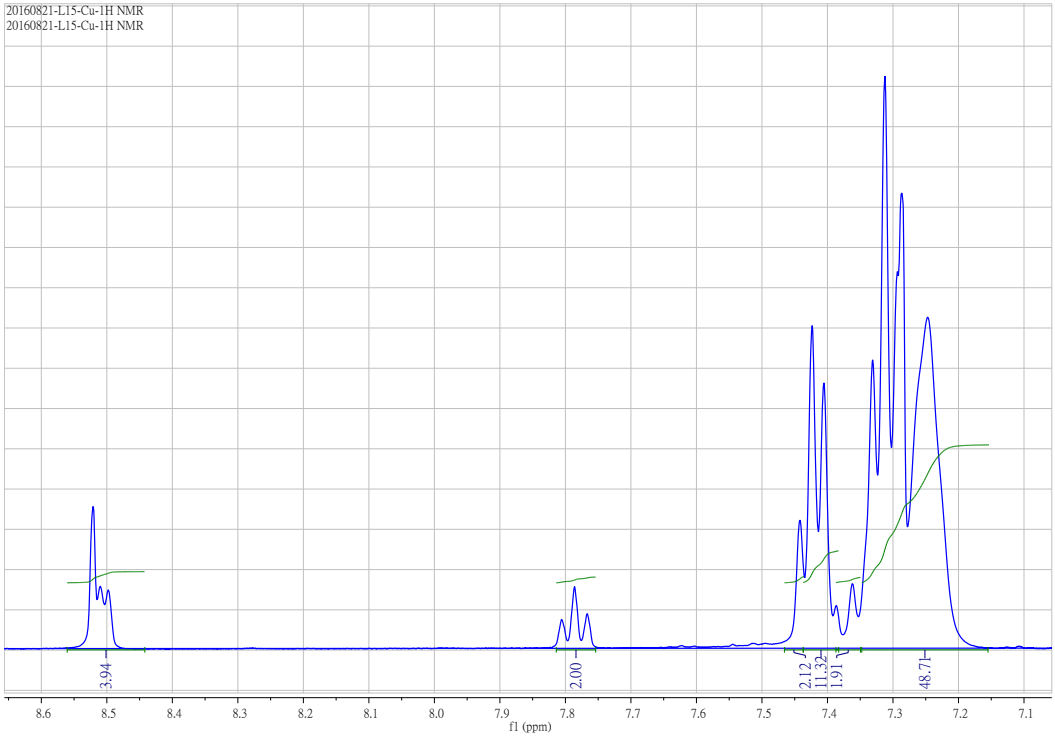

Figure S1. ^{1}H NMR spectroscopy of 1

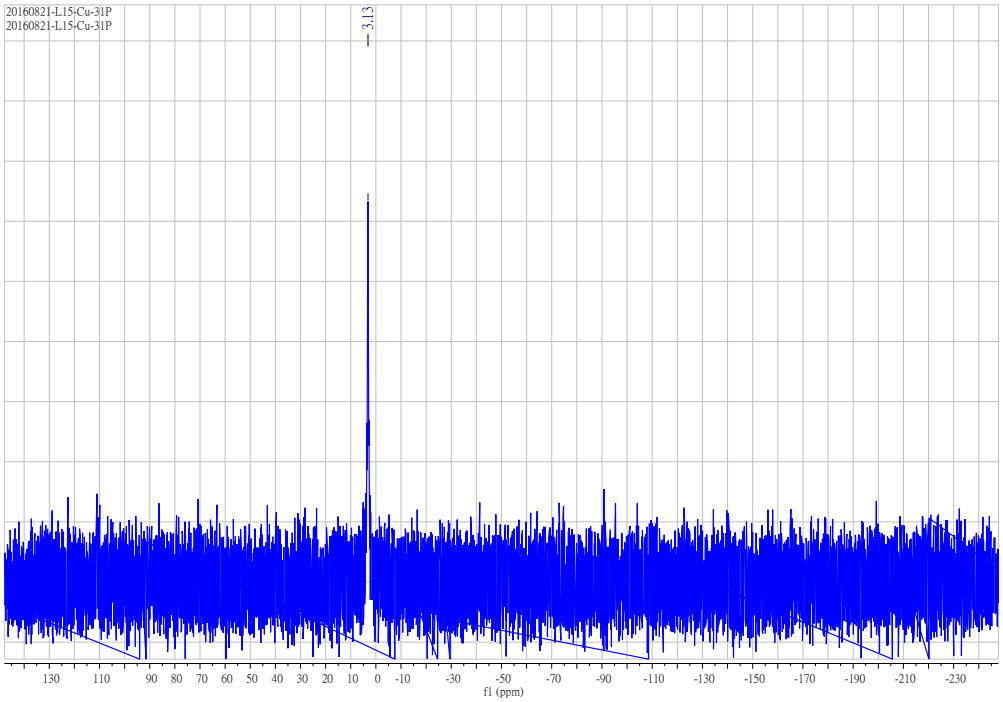

Figure S2. ^{31}P{^{1}H} NMR spectroscopy of 1.

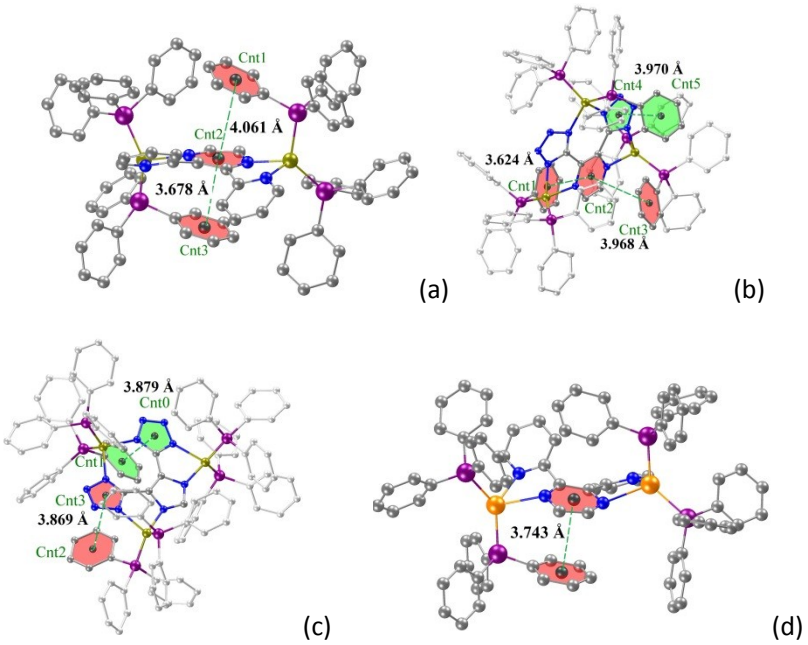

Figure S3. The π···π stacking interactions in **1** (a), **2**(b), **3**(c) and **4** (d).

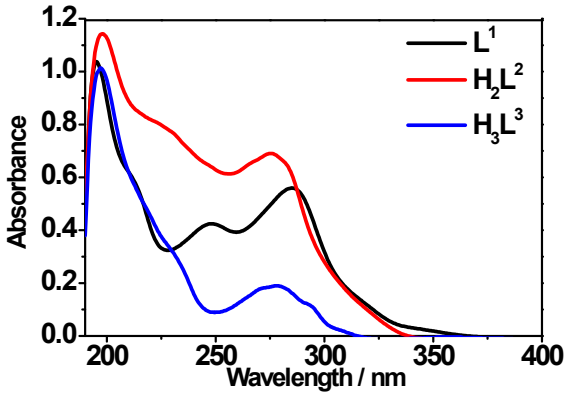

Figure S4. UV spectra of ligands $\mathbf{L^1}$, $\mathbf{H_2L^2}$ and $\mathbf{H_3L^3}$ in MeCN.

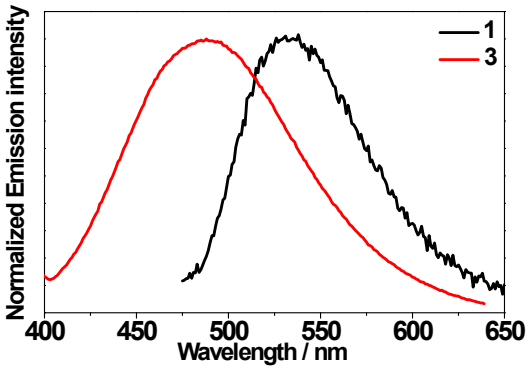

Figure S5. The emission spectra of compounds **1** and **3** in CH_2Cl_2 (λ_{ex} = 400 nm).

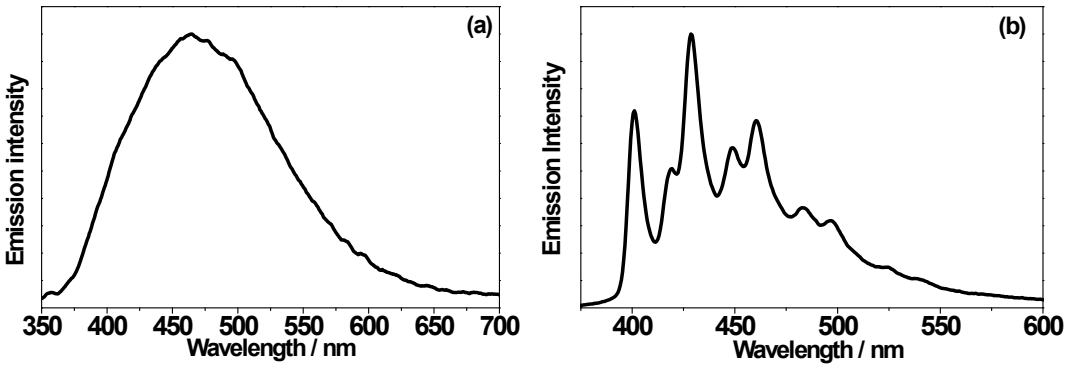

Figure S6. Emission spectra of **3** (a) in solid state and (b) in 77 K EtOH − MeOH (4:1, v/v) glassy state.

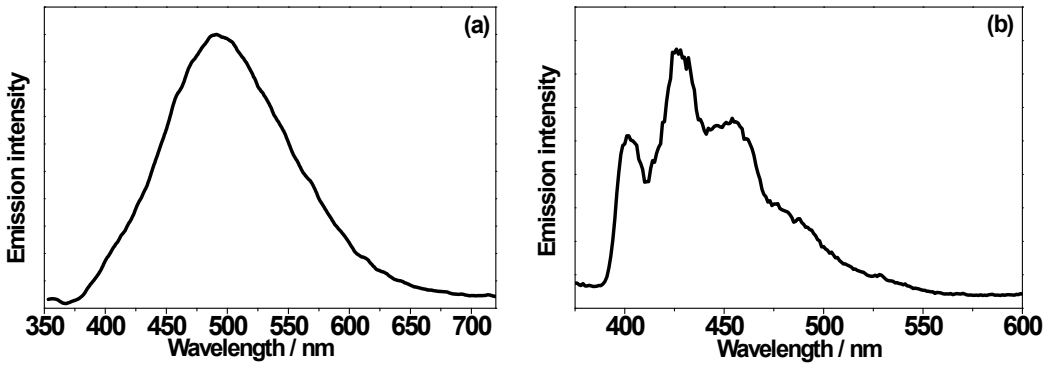

Figure S7. Emission spectra of **6** (a) in solid state and (b) in 77 K EtOH − MeOH (4:1, v/v) glassy state.

Table S1 − **S5.** Calculated transition energies and the changes in the electron densities of the lowest 10 vertical transitions of **1** and **3 – 6.**

Table S1. For compound **1**

λ_{calc} / nm (Oscillator Strength)	**Changes of the electron density (% contribution; H:HOMO, L:LUMO)**	**Transition Characters**
480.25 (0.2049)	**H→L (96.4%)**	MLCT[d(Cu)→π*(**L**^{1})]
455.49 (0.0135)	H-2→L (4.9%), **H-1→L (85.1%)**, H→L+1 (4.7%)	MLCT[d(Cu)→π*(**L**^{1})]
439.50 (0.0067)	H-1→L (3.6%), **H→L+1 (93.2%)**	MLCT[d(Cu)→π*(**L**^{1})]
429.77 (0.0189)	H-4→L (2.8%), **H-2→L (82.9%)**, H-1→L (5.5%)	MLCT[d(Cu)→π*(**L**^{1})]
424.68 (0.0019)	**H-1→L+1 (94.9%)**	MLCT[d(Cu)→π*(**L**^{1})]
415.97 (0.0054)	**H-3→L (87.5%)**, H-3→L+1 (2.8%)	MLCT[d(Cu)→π*(**L**^{1})]
411.70 (0.0256)	**H-4→L (85.5%)**, H-2→L (2.4%)	MLCT[d(Cu)→π*(**L**^{1})]
399.28 (0.0023)	H-9→L (5.2%), H-7→L (21.4%), **H-5→L (56.2%)**, H-4→L+1 (5.6%)	MLCT[d(Cu)→π*(**L**^{1})]
386.48 (0.0014)	H-2→L (2.4%), **H-2→L+1 (92.0%)**	MLCT[d(Cu)→π*(**L**^{1})]
374.82 (0.0001)	H-5→L+1 (2.7%), H-3→L (3.4%), **H-3→L+1 (89.0%)**	MLCT[d(Cu)→π*(**L**^{1})]

Table S2. For compound **3**

λ_{calc} / nm (Oscillator Strength)	Changes of the electron density (% contribution; H:HOMO,L:LUMO)	Transition Characters
344.2 nm (0.0037)	H-1→L+1 (7.9%), H→L (2.2%), **H→L+1 (83.0%)**	LLCT[π(**L³**)→π*(PPh$_3$)] + MLCT[d(Cu)→ π*(PPh$_3$)]
343.0 nm (0.0070)	H-2→L (2.1%), H-1→L (31.5%), **H→L (61.2%)**, H→L+1 (2.5%)	LLCT[π(**L³**)→π*(PPh$_3$)] + MLCT[d(Cu)→ π*(PPh$_3$)]
331.9 nm (0.0055)	H-2→L+1 (14.3%), **H-1→L+1 (38.0%)**, H-1→L+2 (2.1%), **H→L (26.3%)**, H→L+2 (3.0%), H→L+3 (6.0%)	MLCT[d(Cu)→ π*(PPh$_3$)] + LLCT[π(**L³**)→π*(PPh$_3$)]
330.5 nm (0.0045)	H-2→L (2.3%), H-1→L (2.7%), H-1→L+3 (3.1%), H→L (2.9%), H→L+2 (5.9%), **H→L+3 (29.8%)**, **H→L+4 (25.2%)**, H→L+6 (16.0%)	LLCT[π(**L³**)→π*(PPh$_3$)] + MLCT[d(Cu)→ π*(PPh$_3$)]
324.1 nm (0.0227)	H-2→L+2 (7.3%), H-1→L (7.5%), H-1→L+2 (6.7%), H-1→L+4 (3.1%), H→L (4.4%), **H→L+2 (57.5%)**, H→L+3 (2.8%)	LLCT[π(**L³**)→π*(PPh$_3$)] + MLCT[d(Cu)→ π*(PPh$_3$)]
321.6 nm (0.0087)	H-2→L (2.3%), H-1→L (2.7%), H-1→L+3 (3.1%), H→L (2.9%), H→L+2 (5.9%), **H→L+3 (29.8%)**, **H→L+4 (25.2%)**, H→L+6 (16.0%)	LLCT[π(**L³**)→π*(PPh$_3$)] + MLCT[d(Cu)→ π*(PPh$_3$)]
321.2 nm (0.0041)	H-1→L+8 (5.6%), H→L+5 (8.9%), H→L+6 (10.6%), **H→L+7 (49.3%)**, H→L+8 (12.1%)	LLCT[π(**L³**)→π*(PPh$_3$)] + MLCT[d(Cu)→ π*(PPh$_3$)]
319.5 nm (0.0149)	H-1→L+1 (4.5%), H-1→L+3 (2.3%), H-1→L+5 (15.8%), H→L+3 (13.7%), **H→L+5 (40.4%)**, H→L+6 (3.6%), H→L+8 (5.0%), H→L+15 (2.3%)	LLCT[π(**L³**)→π*(PPh$_3$)] + MLCT[d(Cu)→ π*(PPh$_3$)]
317.1 nm (0.0022)	**H-2→L (34.9%)**, H-2→L+2 (8.9%), H-2→L+4 (2.1%), H-1→L (6.6%), H-1→L+5 (3.4%), H→L+2 (15.5%), H→L+3 (2.6%), H→L+6 (2.3%), H→L+7 (2.2%)	MLCT[d(Cu)→ π*(PPh$_3$)] + LLCT[π(**L³**)→π*(PPh$_3$)]
315.9 nm (0.0279)	**H-2→L (34.9%)**, H-2→L+2 (8.9%), H-2→L+3 (2.1%), H-2→L+6 (6.6%), H-1→L+1 (3.4%), H→L+2 (15.5%), H→L+3 (2.6%), H→L+4 (2.3%), H→L+6 (2.2%), H→L+7 (2.2%), H→L+8 (2.2%), H→L+9 (2.2%), H→L+12 (2.2%), H→L+15 (2.2%)	MLCT[d(Cu)→ π*(PPh$_3$)] + LLCT[π(**L³**)→π*(PPh$_3$)]

Table S3. For compound **4**

λ_{calc} / nm (Oscillator Strength)	Changes of the electron density (% contribution; H:HOMO,L:LUMO)	Transition Characters
424.37 nm (0.0282)	**H→L (98.9%)**	MLCT[d(Ag)→π*(**L**^{1})]
396.19 nm (0.0106)	**H-1→L (84.3%)**, H-1→L+1 (7.4%), H→L+1 (6.0%)	MLCT[d(Ag)→π*(**L**^{1})]
393.41 nm (0.0015)	H-1→L (6.1%), **H→L+1 (92.1%)**	MLCT[d(Ag)→π*(**L**^{1})]
388.13 nm (0.0339)	H-3→L (3.4%), **H-2→L (89.3%)**	MLCT[d(Ag)→π*(**L**^{1})]
380.35 nm (0.0056)	H-3→L (11.6%), H-2→L (3.0%), H-2→L+1 (2.3%), H-1→L (5.4%), **H-1→L+1 (75.3%)**	MLCT[d(Ag)→π*(**L**^{1})]
376.20 nm (0.0061)	**H-3→L (70.3%)**, H-3→L+1 (3.4%), H-2→L (2.7%), H-2→L+1 (4.7%), H-1→L+1 (15.3%)	MLCT[d(Ag)→π*(**L**^{1})]
365.57 nm (0.0011)	H-3→L (12.7%), H-3→L+1 (32.9%), **H-2→L+1 (51.4%)**	MLCT[d(Ag)→π*(**L**^{1})]
353.92 nm (0.0005)	**H-3→L+1 (58.5%)**, H-2→L+1 (38.1%)	MLCT[d(Ag)→π*(**L**^{1})]
339.72 nm (0.0173)	H-9→L (3.4%), H-8→L (4.5%), **H-4→L (83.5%)**	LLCT[π(PPh_3)→π*(**L**^{1})]
326.13 nm (0.0158)	**H-21→L (70.3%)**, H-20→L (3.4%), H-19→L (2.7%), H-18→L (4.7%), H-13→L (15.3%), H-6→L (15.3%)	LLCT[π(PPh_3)→π*(**L**^{1})]

Table S4. For compound **5**

λ_{calc} / nm (Oscillator Strength)	**Changes of the electron density (% contribution; H:HOMO,L:LUMO)**	**Transition Characters**
355.0 nm (0.0212)	H-1→L (5.8%), **H→L (93.5%)**	MLCT[d(Ag)→π*(**L²**)]
348.2 nm (0.0056)	H-10→L (2.4%), H-9→L (2.3%), H-2→L (4.2%), **H-1→L (80.7%)**, H→L (5.7%)	MLCT[d(Ag)→π*(**L²**)]
330.7 nm (0.0019)	**H-2→L (87.2%)**, H-1→L (7.3%)	MLCT[d(Ag)→π*(**L²**)] + LLCT[π(PPh_3)→π*(**L²**)]
312.5 nm (0.0050)	H-29→L(2.0%), H-13→L (4.8%), H-11→L (9.7%), **H-10→L (21.9%)**, **H-9→L (24.4%)**, **H-3→L(16.4%)**, H-2→L (7.5%), H-1→L (4.4%)	MLCT[d(Ag)→π*(**L²**)] + LLCT[π(PPh_3)→π*(**L²**)]
304.5 nm (0.0007)	H-11→L (2.2%), H-10→L (6.2%), H-9→L (5.1%), **H-3→L (81.5%)**	MLCT[d(Ag)→π*(**L²**)] + LLCT[π(PPh_3)→π*(**L²**)]
297.1 nm (0.0049)	H-4→L (2.8%), H-1→L+1 (5.9%), **H→L+1 (88.7%)**	MLCT[d(Ag)→π*(**L²**)]
291.7 nm (0.0522)	H-6→L (2.1%), H-5→L (3.4%), **H-4→L (47.4%)**, H-1→L+1 (27.2%), H→L+1 (9.5%)	IL[**L²**] + LLCT[π(PPh_3)→π*(**L²**)]
291.3 nm (0.0148)	H-5→L (2.5%), H-4→L (33.2%), H-2→L+1 (2.3%), **H-1→L+1 (52.8%)**	MLCT[d(Ag)→π*(**L²**)]
285.0 nm (0.0032)	H-13→L (2.3%), H-6→L (3.4%), **H-5→L (79.1%)**, H-4→L (8.4%)	LLCT[π(PPh_3)→π*(**L²**)]
283.3 nm (0.0071)	H-7→L (9.0%), **H-6→L (73.5%)**, H-5→L (4.2%), H-4→L (2.2%), H-2→L+1 (4.8%)	LLCT[π(PPh_3)→π*(**L²**)] + IL[**L²**]

Table S5. For compound **6**

λ_{calc} / nm (Oscillator Strength)	Changes of the electron density (% contribution; H:HOMO,L:LUMO)	Transition Characters
326.98 nm (0.0021)	**H→L (88.4%)**, H→L+1 (8.1%)	LLCT[π(**L**^{3})→π*(PPh_3)]
324.26 nm (0.0009)	H→L (6.0%), **H→L+1 (80.5%)**, H→L+2 (8.9%)	LLCT[π(**L**^{3})→π*(PPh_3)]
321.36 nm (0.0006)	H→L (3.1%), H→L+1 (7.1%), **H→L+2 (81.0%)**, H→L+3 (3.7%)	LLCT[π(**L**^{3})→π*(PPh_3)]
317.33 nm (0.0068)	H→L+3 (3.8%), H→L+4 (20.3%), **H→L+5 (68.8%)**, H→L+6 (3.4%)	LLCT[π(**L**^{3})→π*(PPh_3)]
316.22 nm (0.0094)	**H→L+4 (73.8%)**, H→L+5 (20.0%)	LLCT[π(**L**^{3})→π*(PPh_3)]
314.97 nm (0.0029)	H→L+2 (4.8%), **H→L+3 (89.8%)**, H→L+5 (3.3%)	LLCT[π(**L**^{3})→π*(PPh_3)]
313.37 nm (0.0249)	H→L+4 (2.4%), **H→L+5 (2.4%)**, H→L+6 (88.6%)	LLCT[π(**L**^{3})→π*(PPh_3)]
309.16 nm (0.0077)	**H→L+7 (91.2%)**, H→L+9 (3.2%)	LLCT[π(**L**^{3})→π*(PPh_3)]
305.76 nm (0.0267)	H→L+7 (3.1%), H→L+8 (3.3%), **H→L+9 (87.6%)**	LLCT[π(**L**^{3})→π*(PPh_3)]
303.52 nm (0.0029)	**H→L+8 (95.7%)**, H→L+9 (3.3%)	LLCT[π(**L**^{3})→π*(PPh_3)]

Figure S8. Overlaid experimental (black) and predicted (red) electronic absorption spectra of **3** - **6** in dichloromethane. The predicted vertical transitions were shown as red vertical bars with height equal to their calculated oscillator strengths.